

ON THE TOPIC OF TIME SENSITIVE RECURSIVE OPTIMIZATION OF AN UNDERACTUATED DOCKING MANEUVER

Anthony Aborizk, Bogachan Ondes, and Norman Fitz-Coy

University of Florida, Gainesville, FL, USA

ABSTRACT

The growing prevalence of orbital debris poses a significant hazard to active satellites and space operations. As the risk of cascading collisions increases, the development of reliable autonomous debris removal capabilities becomes crucial. This paper addresses the challenge of autonomous underactuated satellite docking under constrained actuation, with specific focus on small satellite applications in orbital debris remediation. We present an approach to nonlinear Model Predictive Control (MPC) that eliminates the need for terminal constraints and terminal cost to decrease computation time while maintaining a sense of stability. Our method uses the averaged value function to upper bound the nonmonotonic behavior inherent in underactuated systems, providing a more practical and time sensitive alternative to traditional stability requirements. The analysis is conducted on a 6U CubeSat platform with unilateral thrust capability and reaction wheel attitude control, considering both idealized and realistic actuation constraints. We demonstrate through numerical simulations that the proposed control strategy successfully achieves docking objectives with improved computational efficiency. The addition of angular damping is shown to significantly improve system performance under realistic constraints. Our results provide important insights for the development of robust, computationally efficient control strategies for small satellite proximity operations, particularly in the context of orbital debris remediation.

Keywords: Control, Stability, smallsat.

1. INTRODUCTION

The growing prevalence of orbital debris poses a significant hazard to active satellites and other space assets. With over 40,000 objects larger than 10 centimeters being tracked and millions of smaller fragments remaining unmonitored, collisions are an ever-present risk [1]. Fragments significantly smaller than this are untraceable and can travel at speeds high enough to puncture solar panels, damage sensors, or disable vital satellite components. Even a tiny impact can leave a satellite unable

to communicate, maintain power, or hold its orientation, effectively ending its mission. The possibility of cascading collisions—known as Kessler Syndrome [10]—further amplifies the urgency of addressing orbital debris. One cause of orbital debris generation is mission failures. As satellite launches increase, so do the number of mission failures—potentially leading to more debris [2].

However, with the growing interest in space-based technologies, some companies and government organizations have shown interest in developing satellites for the remediation of orbital debris and satellite maintenance [8, 5]. Satellite servicing operations have the potential to extend the life of space-based assets by offering refueling, basic maintenance, repair, and debris removal. However, with what seems to be a growing number of mission failures, it is important to focus on developing systems to prevent satellites from becoming debris—and ensure the service vehicles themselves do not contribute to the problem.

To perform active debris removal, some techniques require the service satellite to dock with the debris item, after which a de-orbiting or relocation process can begin. Given the quantity of debris, automating this process is crucial. This paper focuses on docking with debris items in low Earth orbit using a small-satellite to promote cost efficiency. Additionally, given that many small-satellite mission experience issues post-launch [9], this paper aims to address ways of preventing the service satellite from becoming debris by finding ways to perform docking maneuvers with constrained actuation. The case study presented herein demonstrates a planar underactuated docking problem, wherein a 6U CubeSat is capable of orienting itself about an axis perpendicular to its planar motion and has translation actuation about a unilateral longitudinal axis. Satellite parameters and mission constraints are extensively detailed in this work. While no doubt an interesting problem, it comes with its challenges—various analyses have shown that the formulation of this case study creates a problem that is not controllable or stabilizable at the origin [12, 13]. These notions, of course, rule out the use of many classic feedback approaches, such as Lyapunov’s direct method and linear control theory.

The research herein analyzes an underactuated docking problem with a focus on stability and computational efficiency. Given the control and stability challenges listed

above and Brockett’s condition [6] a stable feedback law can be found, but it cannot be continuous and time invariant. This leaves methods like model predictive control (MPC) (which inherently generates a discontinuous control law), time varying control, control over a manifold, hybrid control, and reinforcement learning as some potential approaches. The analysis herein provides a solution to a benchmark underactuated docking problem—originating from [11]—using nonlinear MPC without terminal constraints or a terminal cost. The negation of these key stability ingredients allows for a reduction in the prediction and control horizon variables, and vastly increases the computational efficiency of the controller. Theorems presented by Grune and Pannek in [7] suggest that stability is not lost with this approach and that methods exist to guide the design of both the prediction horizon variable and the stage cost. While we cannot, at this time, explicitly guarantee stability of this system, we have identified key stability conscious design metrics and have numerically demonstrated our algorithm’s effectiveness. Before presenting our control approach, we first establish the mathematical framework and notation used throughout this paper.

2. PRELIMINARY

2.1. Notation

Vectors are denoted as boldfaced quantities and are defined using the set of real numbers, \mathbb{R}^n , where n is the dimensionality of the space. Matrices will be represented as capital boldfaced quantities. Operations to vectors are coordinatize in the same bases. Vectors will be represented like matrices. The dot product between two vectors $\mathbf{x}, \mathbf{y} \in \mathbb{R}^n$ is written as $\mathbf{x}^T \mathbf{y}$, where \mathbf{x}^T is the transpose of the column vector \mathbf{x} . The magnitude of a vector is calculated using an Euclidean norm function $\|\mathbf{x}\| = \sqrt{x_1^2 + x_2^2 + \dots + x_n^2}$. The time derivative of a vector is denoted with a dot above the variable, $\dot{\mathbf{x}}$, with the number of dots corresponding to the number of differentiations of the variable with respect to time. Variables with an asterisk superscript, x^* , indicate optimal values. A capital calligraphic superscript is used to denote the reference frame a variable is measured in, for example, $\mathbf{x}^{\mathcal{O}}$ is the vector \mathbf{x} measured in \mathcal{O} .

2.2. Equations of Motion

This study looks at two satellites: an uncontrolled cooperative chief in a circular low-Earth orbit and a controlled, but underactuated, 6U CubeSat deputy in Hill’s reference frame. The Hill Clohessy-Wiltshire (HCW) equations linearly represent the relative dynamics between the two satellites with respect to the chief’s frame of reference. This frame is defined by a basis $\mathcal{O} := \{\hat{\mathbf{x}}_{\mathcal{O}}, \hat{\mathbf{y}}_{\mathcal{O}}, \hat{\mathbf{z}}_{\mathcal{O}}\}$, and is fixed to the center of mass of the chief body. The deputy’s body-fixed frame is expressed as $\mathcal{D} :=$

$\{\hat{\mathbf{x}}_d, \hat{\mathbf{y}}_d, \hat{\mathbf{z}}_d\}$ which is aligned with, but separate from, the frame \mathcal{O} .

2.3. Equations of Motions

The linear time-invariant HCW equations can then be used to expressed the location of the deputy in three-dimensional space as follows:

$$\delta \ddot{x} - 3\eta^2 \delta x - 2\eta \delta \dot{y} = \frac{F_x}{m} \quad (1)$$

$$\delta \ddot{y} + 2\eta \delta \dot{x} = \frac{F_y}{m} \quad (2)$$

$$\delta \ddot{z} + \eta^2 z = \frac{F_z}{m} \quad (3)$$

where $\eta = \sqrt{\frac{\mu}{\|\mathbf{x}_c\|^3}}$ is the mean motion of the chief, and F_x , F_y , and F_z represent the thrust magnitude along the $\hat{\mathbf{x}}_o$, $\hat{\mathbf{y}}_o$, and $\hat{\mathbf{z}}_o$ axes, respectively.

Given that the deputy and chief are assumed to be in coplanar orbits, only (1) and (2) will be considered. In other words, $\hat{\mathbf{z}}_o$ -axis effects are not considered. Additionally, since the deputy is underactuated, as seen in Figure 1, the variable F_y defined in (2) is not an explicitly feasible input. However, the following formulation outlines a nonlinear coupling of the deputy’s translational and rotational components, allowing it to still move along the $\hat{\mathbf{y}}_o$ -axis with some additional effort. Let the deputy’s control input be defined as $\mathbf{u}_d := (f_x, \dot{\psi}_z)^T$, where f_x is the thrust magnitude acting along the $\hat{\mathbf{x}}_d$ -axis, and $\dot{\psi}_z$ represents the angular acceleration of the flywheel. The deputy’s state space is defined in Hill’s frame as

$$\mathbf{s} := [x, y, \theta, \dot{x}, \dot{y}, \dot{\theta}]^T$$

where $\mathbf{s} \in \mathbb{R}^6$, x and y are the relative position values measured in meters, \dot{x} and \dot{y} are the relative velocities measured in meters per second, θ is the orientation of the deputy in degrees, and $\dot{\theta}$ is the angular velocity components of the satellite in degrees per second. Note that at $\theta = 0$ deg., the reference frames \mathcal{D} and \mathcal{O} are aligned, but not necessarily concentric. Positive values of θ represent a counterclockwise angular displacement about the $\hat{\mathbf{z}}_o$ -axis, measured from the $\hat{\mathbf{x}}_o$ -axis. The reaction wheel is assumed to be at the center of mass of the deputy with rotations about the $\hat{\mathbf{z}}_d$ -axis. The moments of inertia of the flywheel and the satellite are indicated by D and I_z , respectively. Combining these variables produces an underdamped rotational equation of motion

$$\ddot{\theta} = \frac{-D \dot{\psi}_z}{I_z}. \quad (4)$$

An additional case study is considered in this work wherein damping of the angular variables is considered.

In this case, the angular acceleration of the deputy can be calculated using

$$\ddot{\theta} = \frac{-D\dot{\psi}_z}{I_z} - \frac{c}{I_z}\dot{\theta} \quad (5)$$

where c is the damping coefficient. The additional expressions in (5) are meant to serve as a general representation of damping. With the use of a reaction wheel, c can encompass loss due to internal friction and / or hysteresis. However, if additional damping is required and the deputy is operating in low Earth orbit, for example, a magnetorquer can be used. The angular acceleration equation in this case would become

$$\ddot{\theta} = \frac{-D\dot{\psi}_z}{I_z} - \frac{c}{I_z}\dot{\theta} + \frac{kB}{I_z}u_m$$

where kB is the magnetorquer torque constant and u_m is the control effort. If these additional terms are related to the angular velocity of the deputy, $kBu_m = -kBK\dot{\theta}$ (where K is some additional damping gain), then this term can be consumed by c , and the expression becomes (5).

The state-space form of the HCW equations are given by

$$\dot{\mathbf{s}} = \mathbf{A}\mathbf{s} + \mathbf{B}(\theta)\mathbf{u} \quad (6)$$

$$\mathbf{A} = \begin{bmatrix} 0 & 0 & 0 & 1 & 0 & 0 \\ 0 & 0 & 0 & 0 & 1 & 0 \\ 0 & 0 & 0 & 0 & 0 & 1 \\ 3\eta^2 & 0 & 0 & 0 & 2\eta & 0 \\ 0 & 0 & 0 & -2\eta & 0 & 0 \\ 0 & 0 & 0 & 0 & 0 & 0 \end{bmatrix} \quad (7)$$

$$\mathbf{B}(\theta) = \begin{bmatrix} 0 & 0 \\ 0 & 0 \\ 0 & 0 \\ \frac{\cos(\theta)}{m_c} & 0 \\ \frac{\sin(\theta)}{m_c} & 0 \\ 0 & -\frac{D}{I_z} \end{bmatrix} \quad (8)$$

The mean motion constant, η , represents the average angular rate of the chief. From this formulation, it becomes clear that any actuation in the HCW frame is expressed via a coupling between the angle, θ , and the unilateral thrust, f_x . Therefore, the force expressed in \mathcal{O} is

$$F_{xy} = \begin{bmatrix} \cos(\theta) \\ \sin(\theta) \end{bmatrix} f_x$$

where $F_{xy} = [F_x, F_y]^T$.

3. MODEL PREDICTIVE CONTROL

Model predictive control is a discrete-time finite-horizon recursive optimal control technique. Given some initial

state, \mathbf{s}_0 , measured at time, t_0 , an optimal open-loop control sequence, $\mathbf{u}^* = \{\mathbf{u}_0^*, \mathbf{u}_1^*, \dots, \mathbf{u}_{H-1}^*\}$ with $\mathbf{u}_k^* \in \mathbb{R}^m$, is generated to drive the system to some desired state using an optimal control framework. This optimal control sequence is acquired by minimizing some finite-horizon objective function, J_H , subject to constraints on the dynamics of the system, the state, and the control input.

$$J_H(x_0, u(\cdot)) := \sum_{k=0}^{H-1} l(x_u(k, x_0), u(k)) + F(x_u(H, x_0))$$

To promote stability, a constraint on the terminal state is also used. This is typically formulated as

$$\begin{aligned} V_H &= \min_{\mathbf{x}, \mathbf{u}} J_H(x_0, u(\cdot)) \\ \text{S. T. } u(\cdot) &\in \mathbb{U}^H(x_0), \\ x_u(k+1, x_0) &= f(x_u(k, x_0), u(k)), \\ x_u(0, x_0) &= x_0, \\ x_u(H, x_0) &= 0 \end{aligned} \quad (9)$$

where J_H is the finite horizon objective function, l is the stage cost (or running cost), H is the number of timesteps in the prediction horizon, x_0 is the initial state of the system, $u(\cdot)$ is some arbitrary control sequence, $\mathbb{U}^H(x_0)$ is the allowable input control set when starting from x_0 , x_u is the evolved state space, and $f(x, u)$ is a function describing the evolution of the system. the terminal cost is denoted as $F(x_u(H, x_0))$, and the terminal constraint is denoted as $x_u(H, x_0) = 0$. These components are typically included in what will henceforth be referred to a ‘‘general MPC’’ algorithm to support notions of stability.

3.1. Three Requirements for Stability Without Terminal Cost or Constraints

Theorem 3[7]: Consider the nMPC (9) with optimization horizon $H \in \mathbb{N}$ and running cost l satisfying $\alpha_1(|\mathbf{s} - \mathbf{s}^*|) \leq l^*(\mathbf{s}) \leq \alpha_2(|\mathbf{s} - \mathbf{s}^*|)$ for suitable $\alpha_1, \alpha_2 \in \kappa_\infty$. Suppose the value function is upper bounded by some asymptotic or exponential function and that α from (13) satisfies $\alpha \in (0, 1]$. Then the nominal nMPC closed-loop system with nMPC-feedback law u is asymptotically stable on \mathcal{X} . In addition, the inequality

$$J_\infty(\mathbf{s}, \mu H) \leq \frac{V_H(\mathbf{s})}{\alpha} \leq \frac{V_\infty(\mathbf{s})}{\alpha} \quad (10)$$

holds for each $\mathbf{s} \in \mathcal{X}$

This theorem effectively outlines three requirements for stability of a nonlinear MPC without terminal cost or constraints. First, the running cost must satisfy the following inequality

$$\alpha_1(|\mathbf{s} - \mathbf{s}^*|) \leq l^*(\mathbf{s}) \leq \alpha_2(|\mathbf{s} - \mathbf{s}^*|) \quad (11)$$

for suitable $\alpha_1, \alpha_2 \in \kappa_\infty$. Note that $*$ indicates optimal values. Second, the value function of the MPC must

be upper bounded by some asymptotic function to ensure asymptotic controllability.

$$l(\mathbf{s}_u(n, \mathbf{s}), \mathbf{u}(n)) \leq \beta(l^*(\mathbf{s}), n) \quad (12)$$

Third and finally, the relaxed dynamic programming function

$$V_H(n, \mathbf{s}) \geq \alpha l(n, \mathbf{s}, \mu_H(n, \mathbf{s})) + V_H(n+1, f(\mathbf{s}, \mu_H(n, \mathbf{s}))) \quad (13)$$

must produce an $\alpha \in (0, 1]$. Having established the theoretical foundations of MPC and its stability requirements, we now apply these concepts to our specific satellite docking problem. The following section details how we implement these principles while addressing the unique challenges of underactuated small satellite control.

4. METHODOLOGY

4.1. Equations of Motion

The model used for the deputy in this analysis, depicted in Figure 1, is a 6U CubeSat measuring 30 cm x 20 cm x 10 cm along the \hat{x}_d , \hat{y}_d , and \hat{z}_d -axes, respectively. The satellite can produce thrust unilaterally along the \hat{x}_d -axis (positive and negative). Thrusts are assumed to act through the center of mass of the satellite. The attitude is controlled by a flywheel rigidly attached to the \hat{z}_d -axis of the deputy. The graphics depicted in Figure 1 is taken from [11]. The specific satellite parameters used in this case study are detailed in Table 1 and were selected to match [11].

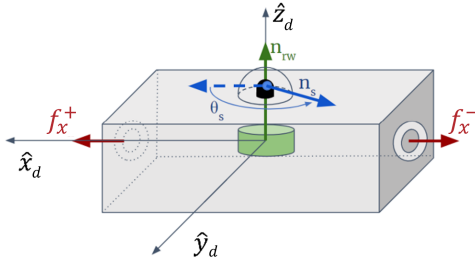


Figure 1. Depiction of the modeled deputy and its body-fixed frame \mathcal{D} . Thrust actuation f_x is aligned along the positive and negative \hat{x}_d -axis. The reaction wheel is depicted in green and its angular momentum vector n_{rw} points along the \hat{z}_d -axis. A gimbaled sensor (black) is affixed to the same axis and has a bore-sight, n_s , and bore-sight angle, θ_s .

Extending the framework of [11], this paper considers an ARPOD case study wherein the deputy must asymptotically dock with the chief while adhering to state and control constraints. The constraints considered exist to simulate realism and ensure safety—they are listed in Table 2.

For realism, limits are placed on the allowable control inputs at any given timestep. These limits exist to emulate the finite capabilities of a thrusters and reaction wheel onboard a 6U CubeSat. Let $f_{x_{min}} = -2 N$ represent the minimum allowable thrust along the negative \hat{x}_d -axis and $f_{x_{max}} = 2 N$ represent the maximum allowable thrust along the positive \hat{x}_d -axis. To ensure the relative velocity is recoverable (i.e., the deputy can be brought to a complete stop within 60 s) this value is bounded at $\pm 10 \frac{m}{s}$. Similarly, bounds are placed on the angular velocity and acceleration as well to ensure safety and to prevent centrifugal damages. Bounds on x and y exist to represent the operating region in which this paper offers analysis.

The constraints presented in [11] were meant to serve as a starting point to a complicated research question. However, the deputy satellite would need to be at least an order of magnitude larger than the 6U CubeSat discussed in this work for these actuation limits to make sense. Therefore, an additional case study is analyzed herein with more appropriate constraint values to further improve realism. These constraints are listed in Table 3. The allowable thrust is decreased from $\pm 2 N$ to $\pm 100 mN$ to represent the higher end of what a 6U CubeSat can accomplish. Similarly, the flywheel angular acceleration limit is decreased to just $\pm 15^\circ/s$ and the velocity is restricted to $\pm 2 m/s$.

4.2. Requirements for Stability

The first requirement for stability from (11) is easily attained. Given that the goal state for the benchmark problem is $\mathbf{0}_6$, the equation becomes

$$\alpha_1(|\mathbf{s}|) \leq l^*(\mathbf{s}) \leq \alpha_2(|\mathbf{s}|).$$

Furthermore, the running cost function can be explicitly defined as

$$l^*(\mathbf{s}) = \mathbf{s}^T \mathbf{Q} \mathbf{s} + \mathbf{u}^{*T} \mathbf{R} \mathbf{u}^*.$$

In other words, the optimal stage cost is a function of the state being acted upon by some optimal control value. Therefore, to satisfy $\alpha_1(|\mathbf{s}|) \leq l^*(\mathbf{s})$, one only needs to remove the control input from the equation,

$$\alpha_1(|\mathbf{s}|) = \mathbf{s}^T \mathbf{Q} \mathbf{s}.$$

However, since the optimal control input, \mathbf{u}^* , is not necessarily always the smallest control input, the upper limit in (11), can be expressed simply as

$$\alpha_2(|\mathbf{s}|) = \mathbf{s}^T \mathbf{Q} \mathbf{s} + \mathbf{u}_{max}^T \mathbf{R} \mathbf{u}_{max}$$

where \mathbf{u}_{max} is a constant maximum absolute bound on the control input such that $\forall u \in \mathcal{U}, |\mathbf{u}| \leq \mathbf{u}_{max}$.

The second and third requirements, however, exist to enforce a monotonically decreasing value function—a requirement that is unfortunately too strict for this problem. Existing research suggests that due to the underactuated nature of this system, there may exist some scenarios

Table 1. Satellite Parameters

Variable	Value	Description
m	12 kg	mass of the deputy
D	$4.1 \times 10^{-5} \text{ kg-m}^2$	reaction wheel spin axis MMoI
I_z	$5.6 \times 10^{-2} \text{ kg-m}^2$	satellite MMoI about the z-axis
η	$1.027 \times 10^{-3} \frac{\text{rad}}{\text{s}}$	mean motion
$ v_{dock} $	$\leq [0.2, 0.2] \frac{\text{m}}{\text{s}}$	maximum docking velocity
$ x_{dock} $	$\leq [0.1, 0.1] \text{ m}$	admissible docking displacement
$ \theta_{dock} $	$\leq 2^\circ$	maximum angular displacement to dock
$ \dot{\theta} $	$\leq 1^\circ/\text{s}$	maximum angular velocity to dock
δt	2 s	timestep

* Mass Moment of Inertia (MMoI). Quantities taken from [11]

Table 2. Case Study 1: Satellite Constraints

Variable	Description
$f_x \in [-2, 2] \text{ N}$	allowable thrust
$\psi \in [-1604, 1604] \frac{\text{deg}}{\text{s}^2}$	allowable flywheel angular acceleration
$x, y \in [-2, 000, 2, 000] \text{ m}$	initial x and y
$\dot{x}, \dot{y} \in [-10, 10] \frac{\text{m}}{\text{s}}$	velocity bounds
$\theta \in [-180, 180] \text{ deg}$	allowable angular values
$\dot{\theta} \in [-2, 2] \frac{\text{deg}}{\text{s}}$	angular velocity bounds
$\ddot{\theta} \in [-1, 1] \frac{\text{deg}}{\text{s}^2}$	bounds on angular acceleration of the deputy

Quantities taken from [11]

where it is beneficial to break this rule [13, 4, 3]. For example, if the system is initialized such that the deputy has a velocity vector pointing away from the chief, and given that constraints on the angular velocity of the deputy must exist, it may be impossible to arrest the initialized motion of the deputy until the satellite is able to reorient itself completely. This could result in the deputy drifting away from the chief during its attitude adjustment, resulting in an increasing value function. To this end, we propose the requirement that the cost decay monotonically is removed and instead replaced with a means of bounding the nonmonotonic tendencies of the system. This is achieved using the average value function.

$$V_H \leq \frac{1}{N} \sum_{n=0}^{N-1} V_{H_n}. \quad (14)$$

With this adjustment, the value function is still forced to decay, but monotonicity is not required. Every N time steps, the average value function is calculated and used as an upper bound for the cost function. This is implemented as a constraint in the optimization loop and is empirically shown to produce faster solving time in the following section. To validate our theoretical framework and demonstrate the effectiveness of the averaged value

function approach, we conducted a series of numerical simulations under both idealized and realistic conditions. The following results demonstrate how our method performs in practice.

5. RESULTS

To demonstrate the feasibility of the MPC method, (14) (henceforth referred to as the averaged value MPC) the underactuated deputy satellite is initialized at the arbitrary initial condition $\mathbf{s}_0 = [3.85, -27.2, -11.1, 0.254, -2.50, 1.25]$. From this initial condition, the the averaged value MPC guides and controls the deputy to the docking configuration—where the admissible docking set is defined by v_{dock} , x_{dock} , θ_{dock} , and $\dot{\theta}$ from Table 1. The resulting trajectory is depicted in Figure 2 and its corresponding value function is depicted in Figure 3. A green circle marks the initial condition in Figure 2. Note that the deputy moves away from the chief at the start of the trajectory before turning around and driving towards the docking configuration. Since the deputy is underactuated the satellite must first orient itself correctly before it can control

Table 3. Case Study 2: Adjusted Satellite Constraints

Variable	Description
$f_x \in [-0.1, 0.1] N$	allowable thrust
$\psi \in [-15, 15] \frac{deg}{s^2}$	allowable flywheel angular acceleration
$x, y \in [-2, 000, 2, 000] m$	initial x and y
$\dot{x}, \dot{y} \in [-2, 2] \frac{m}{s}$	velocity bounds
$\theta \in [-180, 180] deg$	allowable angular values
$\dot{\theta} \in [-2, 2] \frac{deg}{s}$	angular velocity bounds
$\ddot{\theta} \in [-1, 1] \frac{deg}{s^2}$	bounds on angular acceleration of the deputy

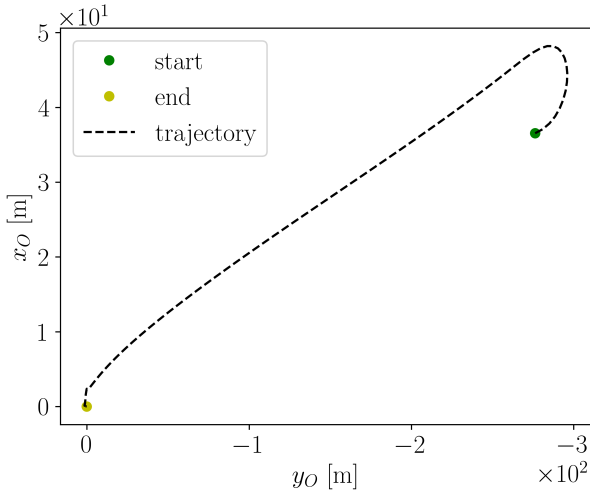


Figure 2. The trajectory generated using the averaged value MPC method. The green circle marks the initial conditions, the yellow circle marks the docking location and the black line shows the trajectory taken.

its translation. Exacerbating this coupled relationship between translation and orientation are the constraints on angular acceleration and angular velocity listed in Table 2. Note that monotonicity was not achieved by this trajectory’s value function in Figure 3. The blue line shows how the value function changes over the course of the trajectory. The orange line shows how the upper bounding averaged value function changes throughout the course of the mission.

Removing the terminal cost constraint from the general MPC algorithm enables us to solve the underactuated docking problem with a smaller horizon, significantly reducing computational time. To maintain stability, we calculate the average value function every N timesteps and use it as an upper bound to the cost function. Figures 4 and 5 compare the performance of both approaches from an arbitrary initial condition $s_0 = [321, -179, 12.5, .396, -1.18, 0.228]^T$. While the general MPC maintains better optimality throughout the trajectory—evidenced by consistently lower value func-

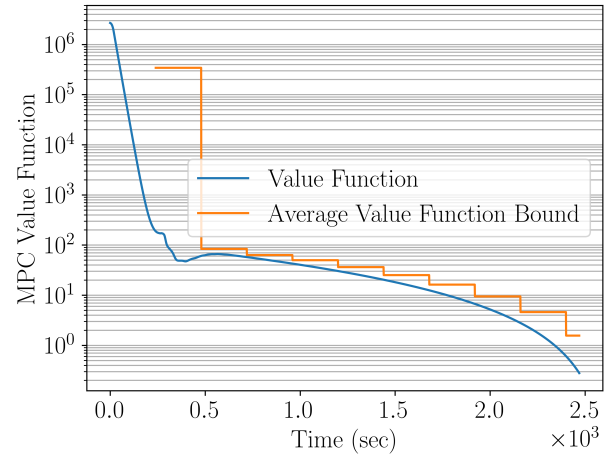


Figure 3. The value function produced by the averaged value MPC method. The blue line shows the value function while the orange line shows its average.

tion values in Figure 5—it comes at a substantial computational cost. Using Python, the general MPC required 17,569 seconds to generate a 275-timestep trajectory, averaging 9.34 seconds of computation per 2-second mission timestep. In contrast, the averaged value MPC completed a longer but feasible 1,676-timestep trajectory in just 971 seconds, averaging 0.58 seconds per timestep. Though this solution is sub-optimal, it remains feasible while achieving a 16-fold reduction in computational time.

While the previous results demonstrate the basic functionality of our approach under idealized conditions, real-world applications require more conservative constraints. To better represent actual 6U CubeSat capabilities, we next analyze the system’s performance under tightened constraints as detailed in Table 3. Figure 6 demonstrates the averaged value MPC scheme’s performance under these tighter constraints. While the algorithm successfully manages nonmonotonic behavior and achieves eventual convergence with the chief, the resulting trajectory exhibits chaotic characteristics. The state-space progression shown in Figure 7 reveals under-damped behav-

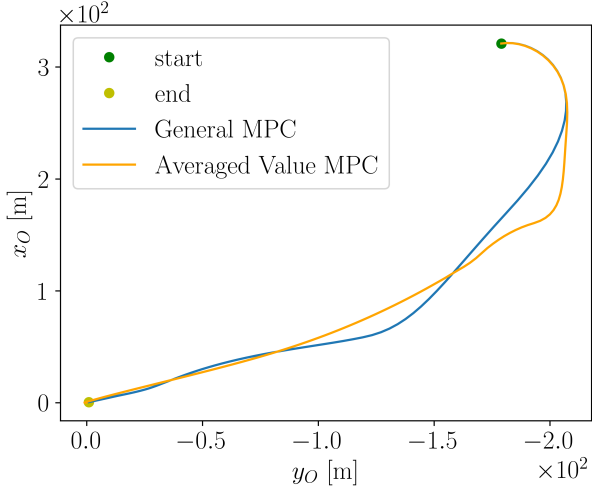


Figure 4. A comparison between the trajectories generated by general MPC in blue and averaged value MPC in orange.

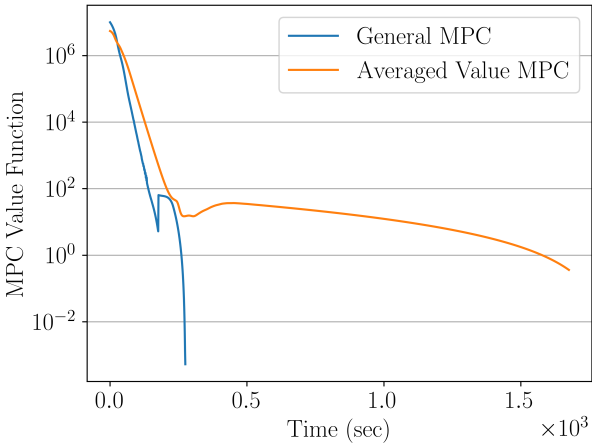


Figure 5. A comparison between the value functions generated by general MPC in blue and averaged value MPC in orange.

ior in the angular variables, characterized by decaying oscillations. Due to the coupled nature of attitude and translation dynamics, these oscillations propagate throughout the entire state space, affecting translational variables as well.

Although additional tuning of this MPC approach might mitigate this chaotic behavior, we instead opted to enhance realism by implementing the damped angular acceleration model (5) rather than the original model (4). With a damping coefficient of $c = 10^{-3}$, Figure 8 shows significantly improved chief-deputy system behavior. The state-space variables in Figure 9 demonstrate complete elimination of the angular oscillations, resulting in smoother overall system performance.

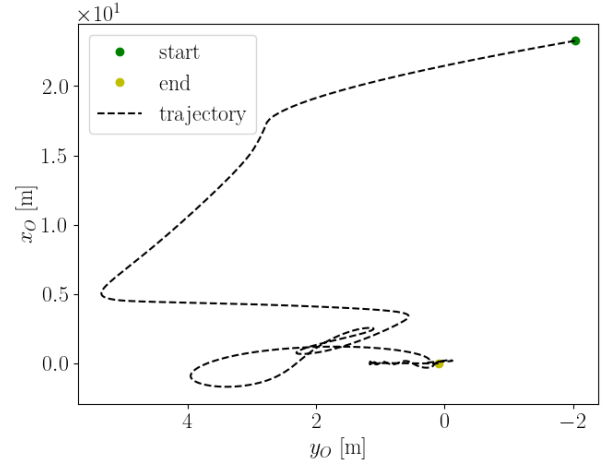


Figure 6. Poorly tuned docking trajectory with realistic constraints on control inputs.

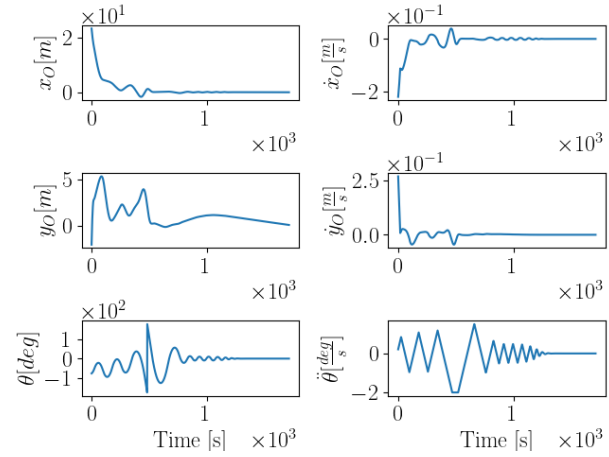


Figure 7. Poorly tuned docking states with realistic constraints on control inputs.

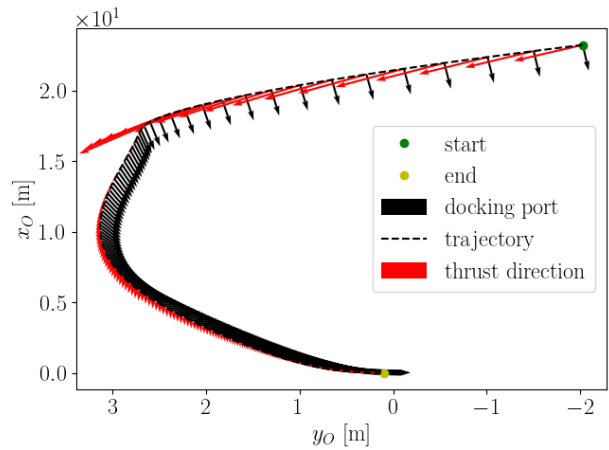


Figure 8. The trajectory produced by the averaged value MPC scheme. The black arrows point in the direction of the deputy's docking port. The red arrows show the direction of thrust.

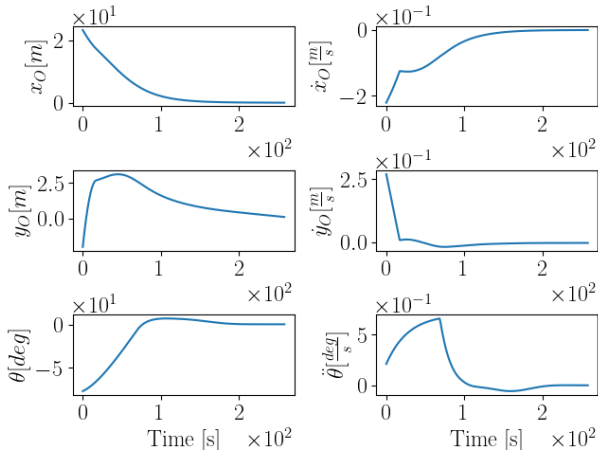


Figure 9. The states produced by the averaged value MPC scheme with damped angular control.

6. CONCLUSION

This paper has presented a computationally efficient MPC approach to autonomous satellite docking under constrained actuation, specifically addressing the challenges faced by small satellites in orbital debris remediation missions. Our primary contribution is the development of an MPC framework that eliminates traditional terminal constraints and costs while maintaining a sense of system stability through an averaged value function approach. This modification achieved a 16-fold reduction in computational time when compared to a conventional MPC method, making it more suitable for real-time implementation on resource-constrained small satellite platforms.

The analysis was conducted using two sets of actuation constraints: an idealized case study and a more realistic scenario representative of actual 6U CubeSat capabilities. When applying realistic constraints, we observed that the coupled nature of attitude and translation dynamics led to oscillatory behavior. This challenge was addressed through the introduction of angular damping, resulting in smoother trajectories and improved overall system performance.

While our approach sacrifices some measure of optimality compared to traditional MPC implementations, it maintains feasibility while significantly reducing computational overhead. This trade-off is particularly relevant for satellite applications, where computational resources are limited and rapid solution generation is crucial for real-time control. Future work could explore the theoretical guarantees of stability under the averaged value function approach and investigate the extension of this method to three-dimensional docking scenarios.

The methods presented here represent a step toward developing practical, computationally efficient control strategies for small satellite proximity operations, particularly in the context of orbital debris remediation. As the

space debris problem continues to grow, efficient and reliable control methods will become increasingly vital for maintaining the long-term sustainability of space operations.

REFERENCES

1. ESA's Annual Space Environment Report. LOG GEN-DB-LOG-00288-OPS-SD, ESA Space Debris Office, ESA ESOC Robert-Bosch-Strasse 5 D-64293 Darmstadt, Germany, July 2024.
2. Mission Success Handbook for Cubesat Missions. Technical Report GSFC-HDBK-8007, NASA Goddard Space Flight Center, Greenbelt, MD, December 2024.
3. Anthony Aborizk, Alexander Soderlund, and Norman Fitz-Coy. An On-Line Global Search Approach to Underactuated Docking Operations Via Model Predictive Control and the Cross-Entropy Method. Darmstadt, Germany, 2024.
4. Anthony Aborizk, Alexander Soderlund, Christopher Petersen, and Norman Fitz-Coy. Nonlinear Model Predictive Control of an Underactuated Small Satellite with Unilateral Thrust. *Journal of Guidance, Control, and Dynamics*, In Processing, 2025.
5. Aaron Avery and David Geller. Dynamic Modeling and Control of an Active Debris Removal Small Satellite. In *AIAA Guidance, Navigation, and Control (GNC) Conference*, Boston, MA, August 2013. American Institute of Aeronautics and Astronautics. ISBN 978-1-62410-224-0. doi: 10.2514/6.2013-4524.
6. R W Brockett. Asymptotic Stability and Feedback Stabilization. In *Differential Geometric Control Theory*, pages 181–191, Cambridge, MA, 1983. Birkhauser Boston.
7. Lars Grüne and Jürgen Pannek. *Nonlinear model predictive control: theory and algorithms*. Communications and control engineering. Springer, Cham, Switzerland, second edition edition, 2017. ISBN 978-3-319-46024-6 978-3-319-46023-9.
8. Chuck Hulme. Final Report of the OSAM-1 Independent Review Board. Technical Report 022729, OSAM-1 / SPIDER Program Manager Program Management Office, February 2024. Section: OSAM-1 (On-Orbit Servicing, Assembly, and Manufacturing 1).
9. Stephen A Jacklin. Small-Satellite Mission Failure Rates. Technical Report NASA/TM—2018–220034, NASA Ames Research Center, Moffett Field, CA, 2019.
10. Donald J Kessler, Nicholas L Johnson, JC Liou, and Mark Matney. The kessler syndrome: implications to future space operations. *Advances in the Astronautical Sciences*, 137(8), 2010. publisher=Citeseer.
11. Christopher D Petersen, Sean Phillips, Kerianne L Hobbs, and Kendra Lang. Challenge Problem:

Assured Satellite Proximity Operations. In *Proc. AAS/AIAA space flight mechanics meeting*, Virtual, 2021.

12. Alexander A. Soderlund and Sean Phillips. Hybrid Systems Approach to Autonomous Rendezvous and Docking of an Underactuated Satellite. *Journal of Guidance, Control, and Dynamics*, 46(10):1901–1918, October 2023. ISSN 0731-5090, 1533-3884. doi: 10.2514/1.G006813.
13. Anonto Zaman, Alexander A Soderlund, Christopher Petersen, and Sean Phillips. Autonomous Satellite Rendezvous and Proximity Operations via Model Predictive Control Methods. Big Sky, Virtual, 2021.